Colloids and Surfaces B: Biointerfaces 125 (2015) 73–81

Contents lists available at ScienceDirect

Colloids and Surfaces B: Biointerfaces

journal homepage: www.elsevier.com/locate/colsurfb

Molybdenum nanoparticles-induced cytotoxicity, oxidative stress, G2/M arrest, and DNA damage in mouse skin fibroblast cells (L929)

Maqsood A. Siddiqui[a,b,*], Quaiser Saquib[a,b], Maqusood Ahamed[c], Nida N. Farshori[d], Javed Ahmad[a,b], Rizwan Wahab[a,b], Shams T. Khan[a,b], Hisham A. Alhadlaq[c,e], Javed Musarrat[a,b], Abdulaziz A. Al-Khedhairy[a,b], Aditya B. Pant[f]

[a] Department of Zoology, College of Science, King Saud University, Riyadh, Saudi Arabia
[b] Al-Jeraisy Chair for DNA Research, King Saud University, Riyadh, Saudi Arabia
[c] King Abdullah Institute for Nanotechnology, King Saud University, Riyadh, Saudi Arabia
[d] Department of Pharmacognosy, College of Pharmacy, King Saud University, Riyadh, Saudi Arabia
[e] Department of Physics and Astronomy, King Saud University, Riyadh, Saudi Arabia
[f] In Vitro Toxicology Laboratory, CSIR–Indian Institute of Toxicology Research, Post Box 80, M.G. Marg, Lucknow, India

ARTICLE INFO

Article history:
Received 31 August 2014
Received in revised form 3 November 2014
Accepted 12 November 2014
Available online 20 November 2014

Keywords:
Molybdenum nanoparticles
Cytotoxicity
Oxidative stress
Cell cycle
DNA damage

ABSTRACT

The present investigation was aimed to study the cytotoxicity, oxidative stress, and genotoxicity induced by molybdenum nanoparticles (Mo-NPs) in mouse skin fibroblast cells (L929). Cells were exposed to different concentrations (1–100 μg/ml) of Mo-NPs (size 40 nm) for 24 and 48 h. After the exposure, different cytotoxicity assays (3-(4, 5-dimethylthiazol-2-yl)-2, 5-diphenyl tetrazolium bromide, MTT; neutral red uptake, NRU; and cellular morphology) and oxidative stress markers (lipid peroxidation, LPO; glutathione, GSH; and catalase) were studied. Further, Mo-NPs-induced intracellular reactive oxygen species (ROS) generation, mitochondrial membrane potential (MMP), cell cycle arrest, and DNA damage were also studied. L929 cells treated with Mo-NPs showed a concentration- and time-dependent decrease in cell viability and a loss of the normal cell morphology. The percentage cell viability was recorded as 25%, 42%, and 58% by MTT assay and 24%, 46%, and 56% by NRU assay at 25, 50, and 100 μg/ml of Mo-NPs, respectively after 48 h exposure. Furthermore, the cells showed a significant induction of oxidative stress. This was confirmed by the increase in LPO and ROS generation, as well as the decrease in the GSH and catalase levels. The decrease in MMP also confirms the impaired mitochondrial membrane. The cell cycle analysis and comet assay data revealed that Mo-NPs induced G2/M arrest and DNA damage in a concentration-dependent manner. Our results demonstrated, for the first time, Mo-NPs induced cytotoxicity, oxidative stress and genotoxicity in L929 cells. Thus, data suggest the potential hazardous nature of Mo-NPs.

1. Introduction

Over the past few years, there is a rapid development in the field of nanotechnology worldwide due to their wide applications in the industry and biomedicine [1]. Nanomaterials possessing novel physical and chemical functional properties have been used in the manufacture of unique devices [2,3]. The major toxicological concerns of these manufactured nanoparticles (NPs) are their distinct properties, such as small size, high number per given mass, large specific surface area, generation of free radicals [4], redox active nature [2], and transportations into mitochondria through the cell membranes [5]. Although, most of the NPs have been shown to induce potential toxicity [6], there is a serious lack of information concerning the impact of these NPs on the environment and the human health. It is well established that NPs can affect different cellular activities [7–9] and can cause toxicity in various organs [10–12]. Numerous studies showed that NPs can cause cytotoxicity, genotoxicity and apoptotic cell death [13–15] through lysosomal membrane destabilization and lipid peroxidation [16]. Although little is known about the mechanism(s) of nanoparticles toxicity, free oxygen radical generation is often used to explain toxicity associated with NPs exposure [17]. Free oxygen radical elicits a wide variety of physiological and cellular events including cellular stress, inflammation, DNA damage, and apoptosis [18]. Many studies have also reported that NPs have the potential to induce

* Corresponding author at: Department of Zoology, College of Science, King Saud University, Riyadh, P.O. Box 2455, Riyadh 11451, Saudi Arabia. Tel.: +966 14699532; mobile: +966 542967835.
E-mail addresses: maqsoodahmads@gmail.com, masiddiqui@ksu.edu.sa (M.A. Siddiqui).

http://dx.doi.org/10.1016/j.colsurfb.2014.11.014
0927-7765/

oxidative damage in cellular components including protein, lipid, and DNA [19,20]. Although a lot of attention has been paid to their potential toxic effects, the mechanism(s) of NPs toxicity are still unclear. Therefore, *in vitro* studies are essential for assessing the toxicity of these nanomaterials. Since molybdenum nanoparticles (Mo-NPs) have a wide range of applications in electron industry, cutting tools, hard alloys, textiles, microelectronic films, coatings, plastics, nanowire, and X-ray tubes. However, till date, there is no report available in the literature on the toxic effects of Mo-NPs. Thus, the L929 mouse skin fibroblast cells have been selected as an *in vitro* model system to study different effects of Mo-NPs. To the best of our knowledge, this is the first study on the cytotoxicity, oxidative stress, and genotoxicity induced by Mo-NPs in L929 cells. The L929 cell line has been well characterized for its relevance to toxicity models [21], as well as for nanotoxicity studies [22–24].

2. Materials and methods

2.1. Reagents and consumables

Molybdenum nanoparticles, and all other specified chemicals, reagents, and diagnostic kits were procured from Sigma Chemical Company Pvt. Ltd., St. Louis, MO, USA, unless otherwise stated. DMEM, antibiotics/antimycotics solution and fetal bovine serum were purchased from Invitrogen, Life Technologies, USA. Culture wares and other plastic consumables used in this study were procured from Nunc, Denmark.

2.2. Cell culture

L929 cells were grown in Dulbecco's modified eagle's medium (DMEM) supplemented with 10% fetal bovine serum (FBS), 0.2% sodium bicarbonate, and antibiotic/antimycotic solution (100×, 1 ml/100 ml of medium). The cells were maintained in 5% CO_2–95% atmosphere under high humidity at 37 °C. Cells were assessed for cell viability by trypan blue dye exclusion assay as described earlier [25], and batches showing more than 98% cell viability were used in this study.

L929 cells were treated with different concentrations of Mo-NPs (1–100 μg/ml) for 24 and 48 h. The treated cells were studied for cytotoxicity assays (MTT and NRU) and cell morphology analysis. Further, oxidative stress markers, i.e. lipid peroxidation (LPO), glutathione (GSH), catalase, reactive oxygen species (ROS) generation, and mitochondrial membrane potential (MMP) were studied. Mo-NPs induced cell cycle arrest and DNA damage were also assessed in L929 cells by flow cytometer and comet assay, respectively. Mo-NPs were suspended in PBS at a concentration of 10 mg/ml and were sonicated at 40 W for 15 min. The stock solution was then diluted in culture medium to reach the desired concentrations for cell treatment.

2.3. Characterization of Mo-NPs

The crystalline nature of Mo-NPs was determined by X-ray diffraction (XRD) pattern. The XRD of Mo-NPs was acquired at room temperature with the help of PANalytical X'Pert X-ray diffractometer equipped with a Ni filter using Cu Kα (k 5 1.54056 Å) radiations as X-ray source. The shape and size of Mo-NPs were determined by field emission transmission electron microscopy (FETEM, JEM-2100F, JEOL, Japan) at an accelerating voltage of 200 kV. Samples for transmission electron microscopy (TEM) analysis were prepared by drop coating Mo-NPs solution on carbon-coated copper TEM grids. The films on the TEM grids were allowed to dry prior to measurement.

2.4. Cytotoxicity by MTT assay

Percent cell viability was assessed using the 3-(4,5-dimethylthiazol-2-yl)-2,5-diphenyl tetrazolium bromide (MTT) assay as described by [26]. Briefly, cells (1×10^4) were allowed to adhere for 24 h in CO_2 incubator at 37 °C in 96 well culture plates. After the exposure, MTT (5 mg/ml of stock in PBS) was added (10 μl/well in 100 μl of cell suspension) in each well and plates were incubated for 4 h in CO_2 incubator at 37 °C. Then, supernatant was discarded and 200 μl of DMSO were added to each well and were mixed gently. The developed color was read at 550 nm. Untreated sets were also run under identical conditions and served as control.

2.5. Cytotoxicity by neutral red uptake (NRU) assay

NRU assay was carried out following the protocol described by [27]. After the exposure, the medium was aspirated and cells were washed twice with PBS, and incubated for 3 h in a medium supplemented with neutral red (50 μg/ml). The medium was then washed off rapidly with a solution containing 0.5% formaldehyde and 1% calcium chloride. Cells were further incubated for 20 min at 37 °C in a mixture of acetic acid (1%) and ethanol (50%) to extract the dye. The plates were read at 550 nm. The values were compared with the control sets.

2.6. Morphological analysis by phase contrast microscope

Morphological changes were observed to determine the alterations induced by Mo-NPs in L929 cells. All the cells were exposed to different concentrations (1–100 μg/ml) of Mo-NPs for 24 and 48 h. The images were taken using an inverted phase contrast microscope at 20× magnification.

2.7. Lipid peroxidation (LPO)

Lipid peroxidation was performed using thiobarbituric acid-reactive substances (TBARS) protocol [28]. Briefly, after the exposure, L929 cells were collected by centrifugation and were sonicated in ice cold potassium chloride solution (1.15%) and were then centrifuged for 10 min at 3000 × *g*. The resulting supernatant (1 ml) was added to 2 ml of thiobarbituric acid (TBA) reagent (15% TCA, 0.7% TBA and 0.25 N HCl) and was heated at 100 °C for 15 min in a boiling bath. Then samples were placed in cold and were centrifuged at 1000 × *g* for 10 min. Absorbance of the supernatant was measured at 550 nm.

2.8. Glutathione (GSH) level

Intracellular GSH level was estimated as described [29]. Briefly, after respective exposure, cells were collected by centrifugation and the cellular protein was precipitated by incubating 1 ml of the sonicated cell suspension with 1 ml TCA (10%) and was placed on ice for 1 h followed by a 10 min centrifugation at 3000 rpm. The supernatant was added to 2 ml of 0.4 M Tris buffer (pH 8.9) containing 0.02 M EDTA, followed by the addition of 0.01 M 5,5′-dithionitrobenzoic acid (DTNB) to a final volume of 3 ml. The tubes were incubated for 10 min at 37 °C in shaking water bath. The absorbance of the yellow color developed was read at 412 nm.

2.9. Catalase activity

The catalase activity in L929 cells exposed to Mo-NPs was assayed following the protocol [30] using H_2O_2 as a substrate.

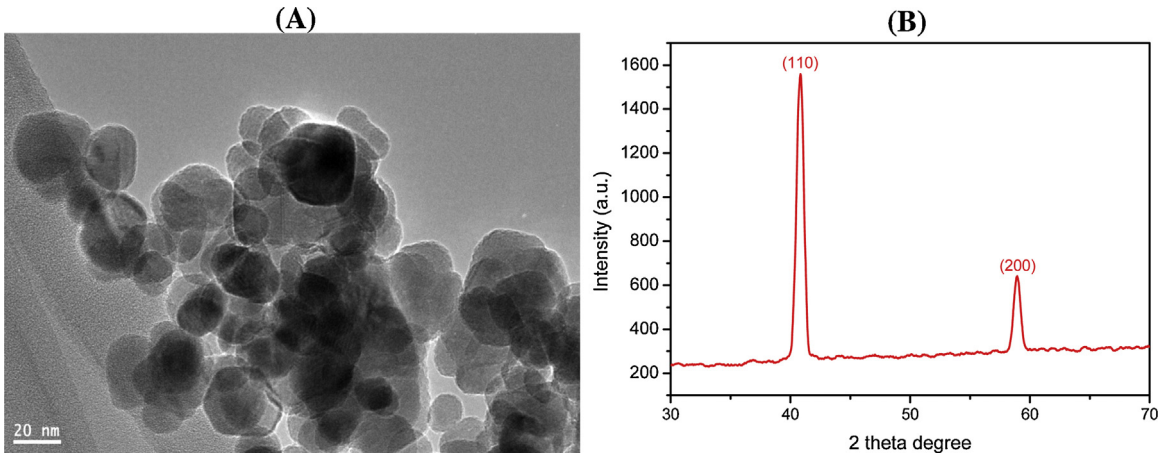

Fig. 1. Characterization of molybdenum nanoparticles (Mo-NPs). (A) Transmission electron microscopy (TEM) and (B) X-ray diffraction (XRD).

Reaction mixture in a final volume of 1 ml consisted of phosphate buffer (pH 7.0), 0.08 μmol of H_2O_2 and enzyme protein. The enzyme activity was measured following disappearance of H_2O_2 at 570 nm.

2.10. Reactive oxygen species (ROS) generation

ROS generation was assessed using 2,7-dichlorodihydrofluorescein diacetate (DCFH-DA; Sigma–Aldrich, USA) dye as a fluorescence agent following the protocol earlier described [15]. Following the exposure of Mo-NPs for 24 h, cells were washed with PBS and were incubated for 60 min in DCFH-DA (20 μM) containing incomplete culture medium in dark at 37 °C. Then, the cells were analyzed for intracellular fluorescence using fluorescence microscope.

2.11. Mitochondrial membrane potential (MMP)

MMP was measured following the protocol of Zhang et al. [31]. In brief, control and treated cells were washed twice with PBS. Then cells were further treated with 10 μg/ml of Rhodamine-123 fluorescent dye for 1 h at 37 °C in dark. Cells were then washed twice with PBS. Then, fluorescence intensity of Rhodamine-123 was measured using fluorescence microscope by grabbing the images at 20× magnification.

2.12. Cell cycle analysis

Cell cycle arrest was determined following the method [14]. In brief, L929 cells were exposed to different concentrations (1–100 μg/ml) of Mo-NPs for 24 h. After the exposure, cells were harvested and centrifuged at 3000 rpm for 5 min. Cell pellets were washed in 500 μl of PBS. Then, cells were fixed with 500 μl of chilled 70% ethanol, and further incubated at 4 °C for 1 h. After two successive washes with PBS at 3000 rpm for 5 min, cell pellets were resuspended in PBS and stained with 50 μg propiodium iodide (PI)/ml containing 0.1% Triton X-100 and 0.5 mg/ml RNAase A for 1 h at 30 °C in dark. Fluorescence of the PI was measured by flow cytometer using Beckman Coulter flow cytometer (Coulter Epics XL/Xl-MCL, Miami, USA) through a FL-4 filter (585 nm). For the measurement, 10,000 events were acquired. The data were analyzed by Coulter Epics XL/XL-MCL, System II Software, Version 3.0. Cell debris characterized by a low FSC/SSC was excluded from the analysis.

2.13. DNA damage by comet assay

DNA strand breaks in L929 cells exposed to different concentrations (10–100 μg/ml) of Mo-NPs for 24 h were quantified by comet assay following the method described [14]. In brief, cells (5×10^4 cells/well) were exposed to Mo-NPs in 24 well plates for 24 h at 37 °C. The cells were washed with serum free medium and were harvested by adding 0.065% trypsin and incubated at 37 °C. The cell suspension was centrifuged at 3000 rpm for 5 min and the pellet was resuspended in 100 μl of PBS. The cells were mixed with 100 μl of 1% LMA and were layered on one-third frosted slides, precoated with NMA (1% in PBS) and kept at 4 °C for 10 min. After gelling, another layer of 90 μl of LMA (0.5% in PBS) was added. The cells were lysed in a lysing solution overnight. After washing with TBE buffer, the slides were subjected to electrophoresis in cold TBE (Tris–base, 90 mM; boric acid, 90 mM; Na_2EDTA, 2.5 mM) buffer. Electrophoresis was performed at 1 V/cm for 30 min (16 mA, 32 V) at 4 °C. All preparative steps were conducted in dark to prevent secondary DNA damage. Each slide was stained with 75 μl of 20 μg/ml ethidium bromide solution for 5 min. The slides were analyzed at 40× magnification (excitation wavelength of 515–560 nm and emission wavelength of 590 nm) using a fluorescence microscope (Nikon Eclipse 80i, Japan) coupled with a charge coupled device (CCD) camera. Images from 100 cells (50 from each replicate slide) were randomly selected and subjected to image analysis using software Comet Assay IV (Perceptive Instruments, Suffolk, UK).

2.14. Statistical analysis

Results were expressed as mean ± standard error of three independent experiments (each in triplicate). Statistical analysis was performed using one-way analysis of variance (ANOVA) post hoc Dunnett's test was applied to compare values between control and treated groups. The values depicting $p < 0.05$ were considered as statistically significant.

3. Results

3.1. Characterization of molybdenum nanoparticles

Fig. 1(A) shows the typical TEM image of Mo-NPs. The average diameter was calculated from measuring over 100 particles in random fields of TEM view. The average TEM diameter of Mo-NPs was 40 nm. Fig. 1(B) shows the XRD pattern of Mo-NPs that clearly exhibits the crystalline nature of this material. The

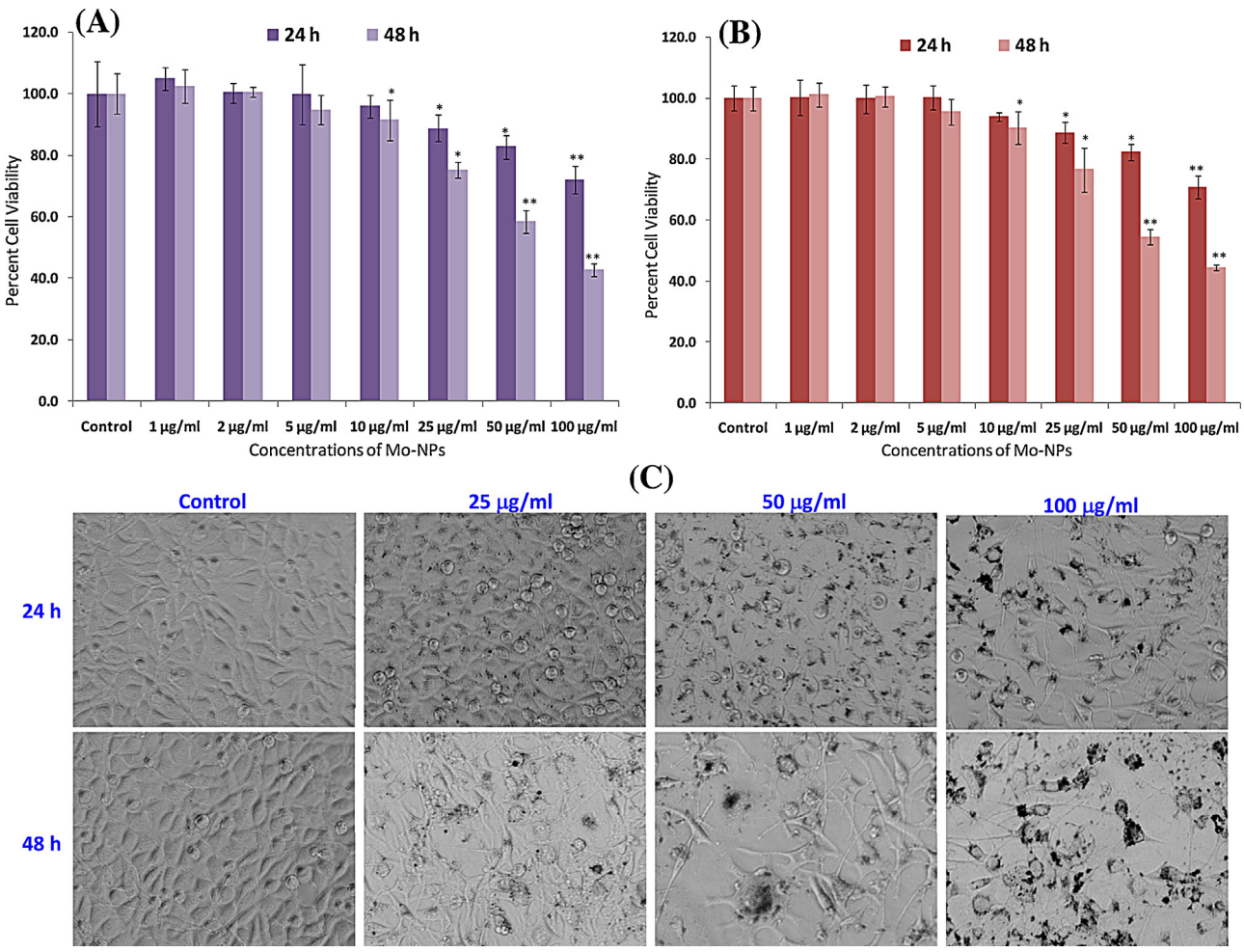

Fig. 2. Cytotoxicity assessment by (A) MTT assay. (B) NRU assay. (C) Morphological changes in L929 cells following the exposure of various concentrations of molybdenum nanoparticles for 24 and 48 h. Images were taken using an inverted phase contrast microscope at 20× magnification. $^{*}p < 0.01$, $^{**}p < 0.001$ vs control.

crystalline size has been estimated from the XRD pattern using the Scherrer's equation [32]. The average crystalline size of Mo-NPs was also found to be 40 nm which is supporting the TEM data.

3.2. Cytotoxicity assessment (MTT assay)

Highlights of the results of the MTT assay are summarized in Fig. 2(A). A concentration and time dependent statistically significant ($p < 0.001$) decrease in percentage cell viability of L929 cells was recorded following 24 and 48 h exposure of Mo-NPs. Cell viability at 25, 50, and 100 μg/ml of Mo-NPs exposed for 24 h were recorded as 12%, 18%, and 28%, respectively. A chronological further decrease in percentage cell viability was also observed at extended exposure period of 48 h, that is, 25%, 42%, and 58% for 25, 50, and 100 μg/ml of Mo-NPs, respectively. A significant decrease at 10 μg/ml of Mo-NPs exposed for 48 h was observed, but Mo-NPs exposed cells for 24 h at 10 μg/ml and lower concentrations did not cause any significant decrease in cell viability (Fig. 2A).

3.3. Cytotoxicity by NRU assay

Data highlights of NRU assay are summarized in Fig. 2B. A concentration and time dependent statistically significant ($p < 0.001$) decrease in cell viability of L929 cells was also recorded following the exposure of Mo-NPs for 24 and 48 h. Percent cell viability at 25, 50, and 100 μg/ml of Mo-NPs exposed for 24 h were recorded as 13%, 17%, and 30%, respectively by NRU assay. At 48 h exposure, the cell viability was recorded as 24%, 46%, and 56% for 25, 50, and 100 μg/ml of Mo-NPs, respectively. Like MTT assay, a significant decrease at 10 μg/ml of Mo-NPs exposed L929 cells for 48 h was observed, but Mo-NPs exposed cells for 24 h at 10 μg/ml and lower concentrations did not cause significant decrease in the cell viability of L929 cells (Fig. 2B).

3.4. Morphological changes

The morphological changes observed in L929 cells exposed to Mo-NPs for 24 and 48 h are shown in Fig. 2C. Alterations in the morphology of L929 cells were observed under phase contrast inverted microscope. The cells indicate the most prominent effects after the exposure of Mo-NPs and changes in their morphology, which were found to be concentration and time dependent. L929 cells exposed to 25 μg/ml and higher concentrations of Mo-NPs reduced the normal morphology of the cells and cell adhesion capacity as compared to control. Most of the cells exposed to 100 μg/ml of Mo-NPs for 48 h lost their typical morphology.

3.5. Lipid peroxidation

The Mo-NPs induced lipid peroxidation in L929 cells exposed for 24 and 48 h are summarized in Fig. 3A. A concentration and time dependent significant increase in the lipid peroxidation

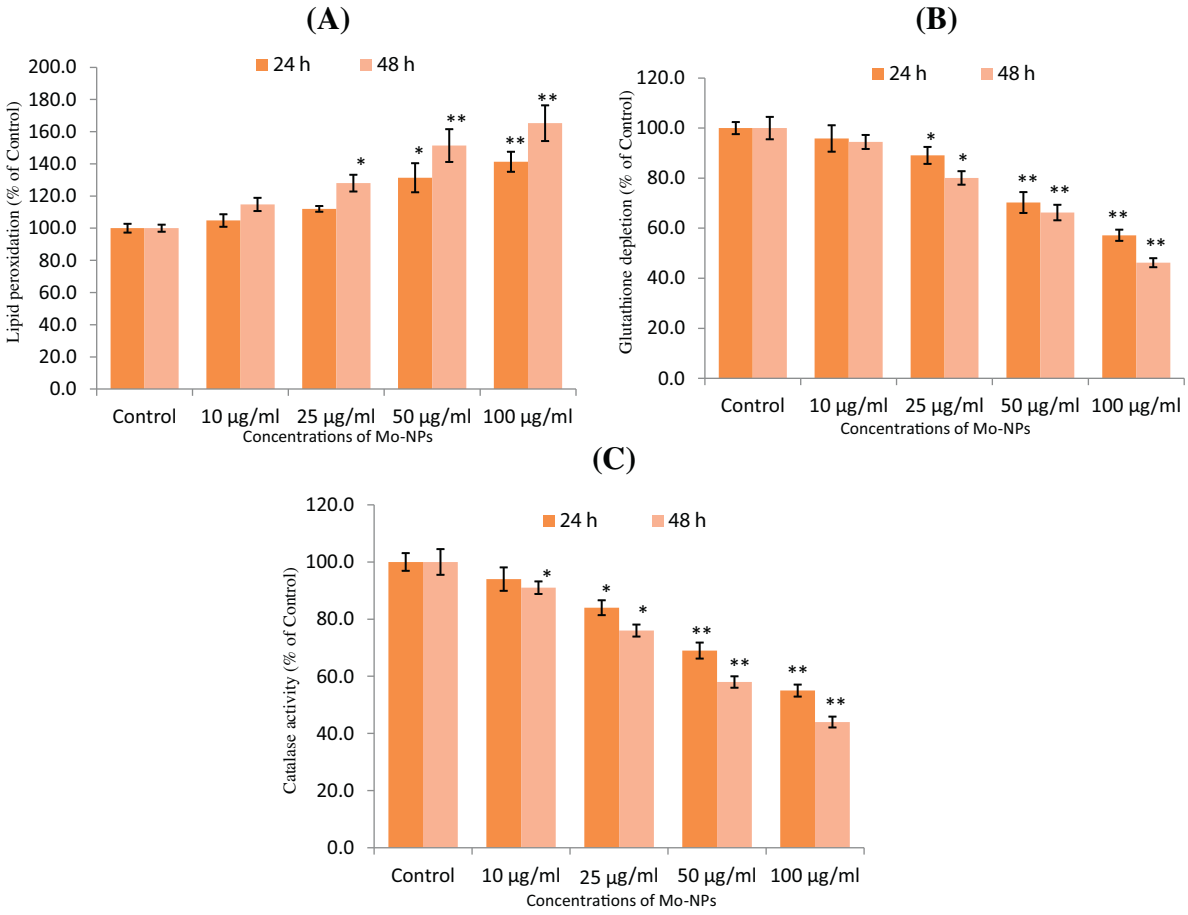

Fig. 3. Molybdenum nanoparticles induced oxidative stress in L929 cells exposed for 24 and 48 h. (A) Lipid peroxidation. (B) Glutathione depletion. (C) Catalase activity. $^{*}p < 0.01$, $^{**}p < 0.001$ vs control.

was observed. An increase of 12%, 31%, and 41% at 25, 50, and 100 μg/ml of Mo-NPs, respectively were observed in L929 cells exposed for 24 h. At 48 h, an increase in the LPO level was observed as 28%, 51%, and 65% at 25, 50, and 100 μg/ml of Mo-NPs, respectively.

3.6. Glutathione depletion

The results of depletion in the glutathione level in cultured L929 cells exposed to 1–100 μg/ml concentrations of Mo-NPs for 24 and 48 h are summarized in Fig. 3B. The results indicated that Mo-NPs decreased the GSH levels in a concentration and time dependent manner. A significant decrease in GSH level was observed as 11%, 30%, and 43% and 55% at 25, 50, and 100 μg/ml, respectively in Mo-NPs exposed L929 cells for 24 h as compared to untreated control. Whereas, decreases of 20%, 34%, and 54% in GSH level was observed at 25, 50, and 100 μg/ml, respectively in Mo-NPs exposed cells for 48 h.

3.7. Catalase activity

The results of catalase activity in L929 cells exposed to Mo-NPs are summarized in Fig. 3C. A concentration and time dependent decrease in catalase activity was also observed in L929 cells exposed for 24 and 48 h. A significant decrease of 16%, 31%, and 45% was observed at 25, 50, and 100 μg/ml of Mo-NPs, respectively. Whereas, the decrease in catalase activity at 25, 50, and 100 μg/ml of Mo-NPs exposed cells for 48 h recorded 24%, 42%, and 56%, respectively as compared to untreated control.

3.8. ROS generation

A statistically significant ($p < 0.001$) ROS generation was observed in L929 cells exposed to Mo-NPs at 25, 50, and 100 μg/ml concentrations for 24 h (Fig. 4A and B). The increase in ROS generation was observed in a concentration dependent manner, i.e., 13%, 51%, and 89% of untreated control following the exposure of 25, 50, and 100 μg/ml of Mo-NPs, respectively.

3.9. Mitochondrial membrane potential

The effect of Mo-NPs exposure on mitochondrial membrane potential (MMP) was evaluated in L929 cells. A concentration dependent statistically significant ($p < 0.001$) decrease in the level of MMP was observed in L929 cells after the exposure of Mo-NPs for 24 h. The decrease in MMP were observed to be 9%, 29%, and 60% at 25, 50, and 100 μg/ml of Mo-NPs, respectively as compared to untreated control (Fig. 5A and B).

3.10. Cell cycle analysis

Flow-cytometric analysis of cell cycle progression in L929 cells exposed for 24 h are summarized in Fig. 6. Data revealed the significant G2/M arrest in L929 cells after the exposure of different concentrations (1–100 μg/ml) of Mo-NPs for 24 h. Cell cycle analysis of propiodium iodide stained control and Mo-NPs treated cells indicated an increase in apoptotic G2/M peak. A significant increase of 31.8%, 42.2%, and 47.6% in G2/M phase was observed at 25, 50, and 100 μg/ml, respectively in Mo-NPs exposed L929 cells for 24.

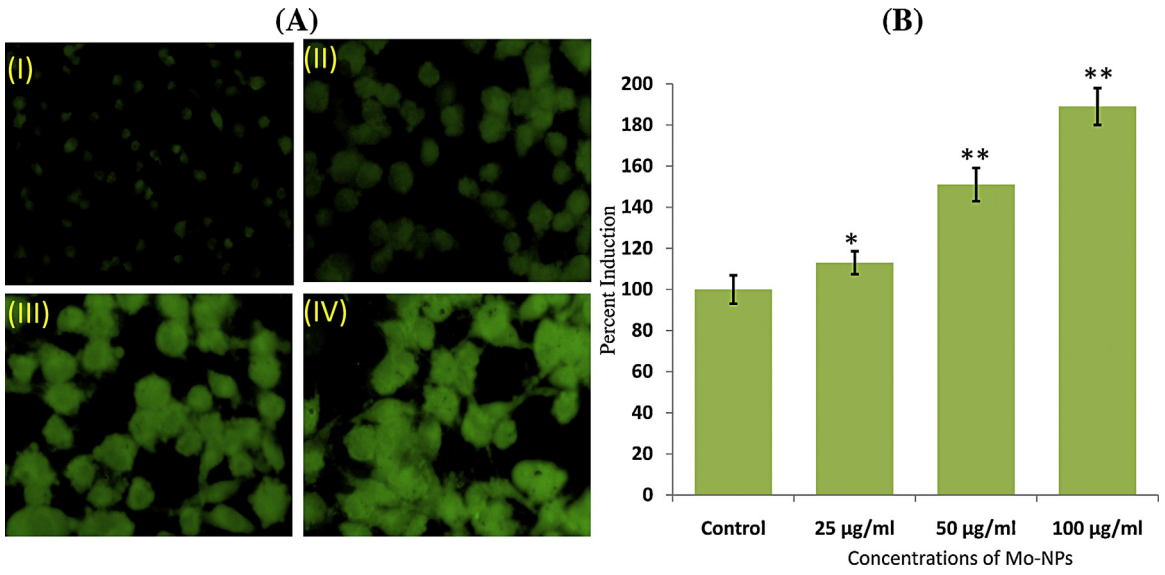

Fig. 4. (A) Molybdenum nanoparticles induced ROS generation in L929 cells. ROS generation was studied using dichlorofluorescindiacetate (DCFH-DA) dye after the exposure of molybdenum nanoparticles for 24 h. (I) Control; (II) 25 μg/ml; (III) 50 μg/ml; and (IV) 100 μg/ml. (B) Percent induction of ROS generation in L929 cells following the exposure of various concentrations of molybdenum nanoparticles for 24 h. $^{*}p < 0.01$, $^{**}p < 0.001$ vs control.

3.11. DNA damage by comet assay

The L929 cells exposed to Mo-NPs for 24 h have exhibited significant induction of DNA damage in a concentration dependent manner as compared to control cells in the standard alkaline comet assay as measured by the comet assay parameters i.e., olive tail moment (OTM), tail length, and % tail DNA intensity (Table 1). The representative images of DNA damage obtained by the comet assay are shown in Fig. 7A and B. The cells treated with 10, 25, 50, and 100 μg/ml of Mo-NPs for 24 h exhibited 24-, 40-, 78-, and 114-fold higher OTM values, as compared to the untreated control (Table 1). An increase in tail length (2.1-, 2.4-, 2.8-, and 3.3-fold at 10, 25, 50, and 100 μg/ml, respectively) and % tail DNA (9.9-, 15-, 23.2-, 27.7-fold at 10, 25, 50, and 100 μg/ml, respectively) was also observed in L929 cells exposed for 24 h (Table 1).

Table 1
Mo-NPs induced DNA damage in L929 cells after 24 h of exposure, analyzed using different parameters of alkaline comet assay.

Groups	Olive tail moment (arbitrary unit)	Tail length (μm)	Tail intensity (%)
Control	0.39 ± 0.06	33.04 ± 2.74	3.30 ± 0.44
EMS (1 mM)	30.41 ± 0.14**	89.30 ± 0.80**	81.96 ± 0.27**
Mo-NPs (μg/ml)			
10	9.33 ± 0.43**	71.94 ± 1.97**	32.63 ± 1.12**
25	15.67 ± 3.42**	80.50 ± 2.39**	49.50 ± 8.37**
50	30.66 ± 3.16**	93.91 ± 4.83**	76.71 ± 2.77**
100	44.42 ± 1.89**	109.69 ± 2.83**	91.42 ± 1.26**

Data represent the mean ± S.D. of three independent experiments done in duplicate. EMS: ethyl methanesulphonate. Statistical analysis was performed by one-way analysis of variance (ANOVA) using Dunnett's multiple comparisons test. The level of statistical significance chosen was $p < 0.05$, unless otherwise stated.
** $p < 0.01$ vs control.

4. Discussion

Characterization of nanoparticles (NPs) is essential in the nanotoxicology research for a better interpretation of the results

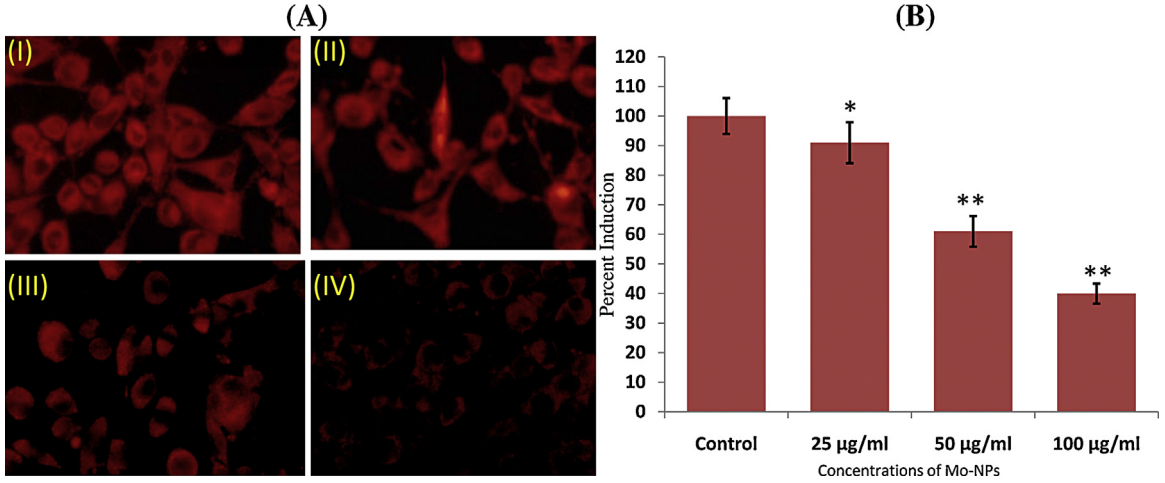

Fig. 5. (A) Molybdenum nanoparticles induced reduction in the intensity of mitochondrial membrane potential (MMP) in L929 cells exposed for 24 h. MMP was studied using Rh123 fluorescent dye. (I) Control; (II) 25 μg/ml; (III) 50 μg/ml; and (IV) 100 μg/ml. (B) Percent induction of MMP in L929 cells following the exposure of various concentrations of rotenone for 24 h. $^{*}p < 0.01$, $^{**}p < 0.001$ vs control.

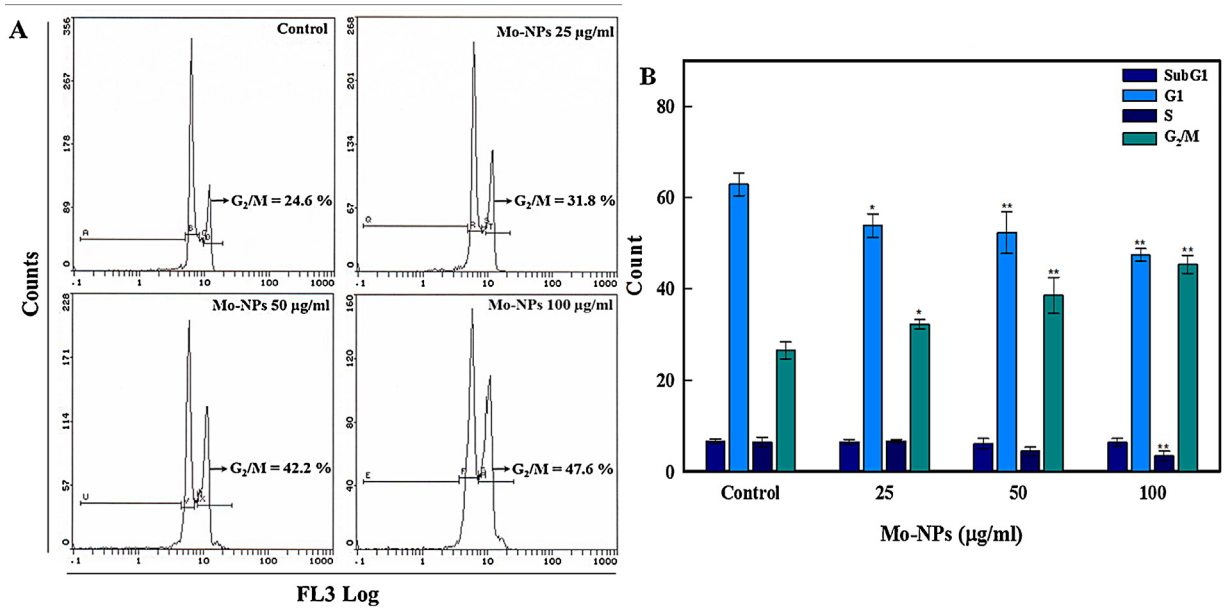

Fig. 6. Cell cycle analysis in L929 cells exposed to different concentrations of Mo-NPs for 24 h. (A) Representative flow cytometric image exhibiting changes in the progression of cell cycle. G2/M in each micrograph represent the percentage of cells in the G2/M phase. (B) Each histogram represents the percentage of cells arrested in different phases of cell cycle. $^{*}p < 0.05$, $^{**}p < 0.001$ vs control.

[33–35]. In this study, characterization was performed using XRD and TEM in order to provide crystalline nature, morphology and particle size of Mo-NPs. Our XRD results confirm the crystalline nature of Mo-NPs. TEM analysis showed that Mo-NPs are spherical in shape with a smooth surface and have an average diameter of 40 nm. Cytotoxicity assessments by MTT and NRU assays revealed a concentration and time dependent decrease in the cell viability of L929 cells exposed to Mo-NPs for 24 and 48 h at 10–100 μg/ml. There is no literature available on molybednum nanoparticles cytotoxicity till date. In one of the studies, Hussain et al. [36] showed that molybdenum trioxide (MoO_3) exposure did not produce cytotoxicity up to 100 μg/ml concentration in BRL 3A rat liver cells. However, in another study, they showed that MoO_3 exerts toxic effects on cellular metabolic activity at 50 μg/ml and at the higher concentrations with an EC_{50} of 90 μg/ml in mammalian germline stem cells [37]. Our cytotoxicity results are in well agreement with the previous findings showing a decrease in the cell viability within this concentration range by the exposure to different NPs including, nickel ferrite NPs in A549 cells [38], silica NPs in HepG2 cells [39], nickel oxide NPs in MCF-7 and HEp2 cells [9], and copper oxide NPs in human liver and lung epithelial cells [8,15]. Our results also correlate well with the recent reports on nanoparticles induced loss of mitochondrial potential and lysosomal membrane destabilization [14,40,41]. The morphological changes in L929 cells exposed to Mo-NPs also confirms the cytotoxic effects as observed by the detachment of the adherent cells, and the reduced morphology with increasing concentrations. These kinds of morphological changes have been also observed in nanoparticles exposed cells by various investigators [15,37,42]. Oxidative stress has been cited to be one of the most important mechanisms of toxicity induced by nanoparticles exposure [9,15,43]. Results from this study also showed that Mo-NPs induced oxidative stress in L929 cells in a concentration and time dependent manner, that is, an increase in the level of lipid peroxidation and a decrease in the antioxidant enzyme GSH level as well as catalase activity. These studies suggest that oxidative stress may be the primary mechanism of toxicity in mouse skin fibroblast cell line (L929) induced by Mo-NPs. Our results are also supported by the previous findings suggesting that the cytotoxicity of Mo-NPs is mediated through the oxidative stress [44,45]. Reactive oxygen species (ROS) are continuously generated through normal cellular metabolisms or by exogenous insults. In this study, we observed Mo-NPs induced intracellular ROS generation in a concentration-dependent manner. Similar to other oxidative stress markers, ROS production was also significantly higher in L929 cells, since the excess generation of ROS has been considered as a crucial mediator of cell death [46]. We also found a decrease in the mitochondrial membrane potential (MMP) in L929 cells exposed to Mo-NPs. The decrease in the MMP, based on cationic fluorescent probe Rh123, indicates the role of oxidative stress in toxicity of Mo-NPs. As shown in Fig. 5A and B, the MMP decreases in a dose-dependent manner, which is in well agreement with Dornetshuber et al. [47], suggesting a less preserved mitochondrial integrity. The lesser fluorescence intensity of Rh123 in Mo-NPs exposed L929 cells might be due to the oxygen radicals production during mitochondrial respiration, suggesting a possible correlation between oxidative stress and mitochondrial activity [48]. From the present study, the results confirmed that Mo-NPs activate the G2/M cell cycle checkpoint. The flow-cytometric analysis of 24 h treated L929 cells suggests the activation of DNA repair process with a noticeable cell cycle arrest in G2/M phase in damaged cells at 25, 50, and 100 μg/ml concentration of Mo-NPs. It is known that the cellular DNA repair mechanisms are highly conserved [49] and that the extensive DNA damage may lead to cell-cycle arrest and cell death as observed in this study. Our data also exhibit that the Mo-NPs inhibited L929 cells proliferation by inducing G2/M arrest (Fig. 6). The G2/M phase has played an important role in mitotic processes. G2/M DNA damage checkpoint serves to prevent cells from entering mitosis (M-phase) with genomic DNA damage [50–52]. Several studies also demonstrated that NPs suppress the progression of cell cycle in different cells [53–55].

We studied the genotoxic potential of Mo-NPs in L929 cells in the alkaline comet assay, which is capable of detecting single as well as double DNA strand breaks and alkali labile sites. The results showed that Mo-NPs induced concentration dependent highly significant DNA damage as observed by the induction in the fold change of olive tail moment (OTM), percent tail DNA, and tail length as shown in Fig. 7A and B and Table 1. The DNA damage caused by Mo-NPs can be explained on the basis of the experimental evidence of genotoxic effect. Due to the small size, high number per

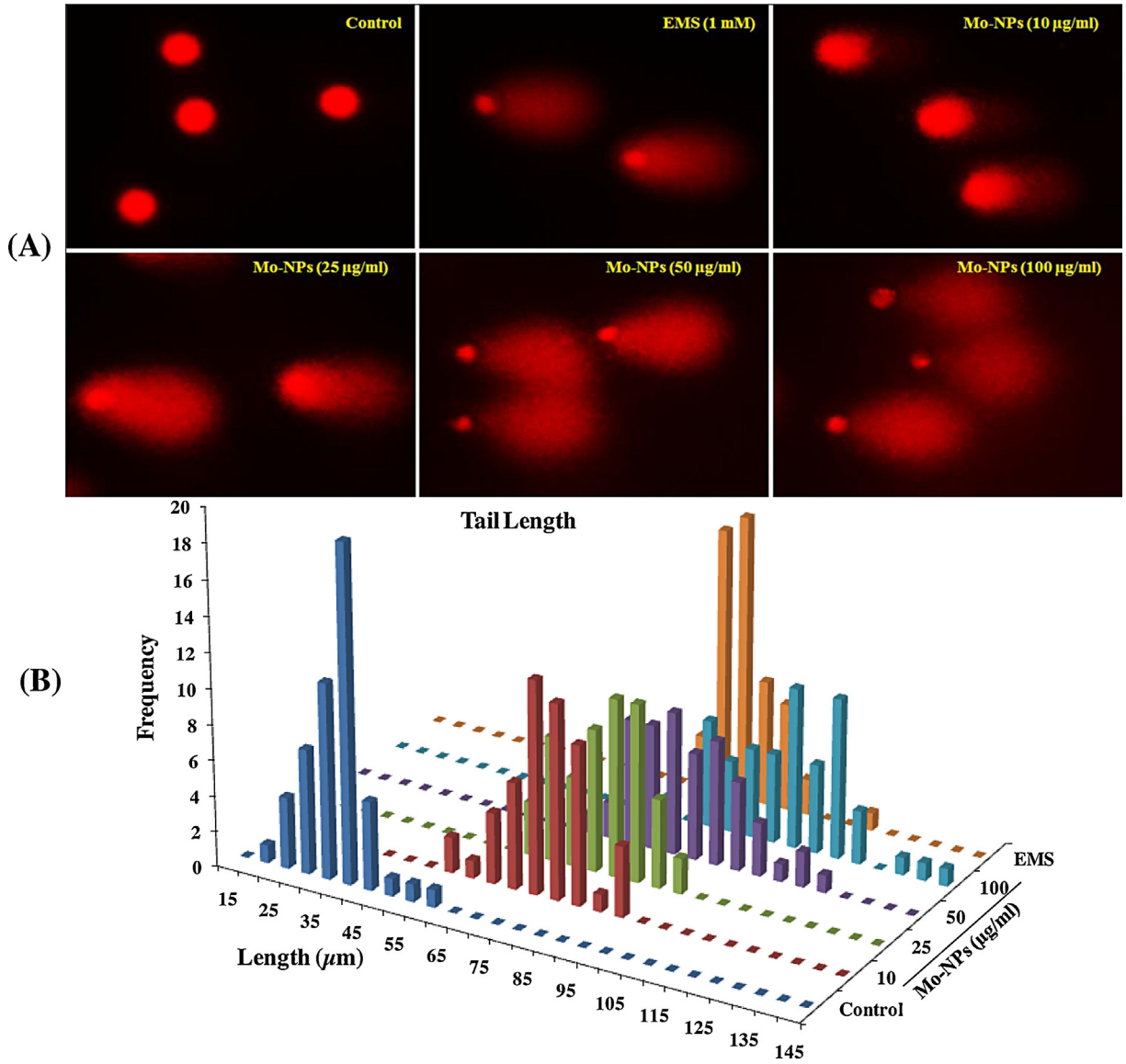

Fig. 7. Mo-NPs induced strand breaks in cellular DNA of L929 cells. (A) Representative epi-fluorescence images of DNA damage by comet assay. (B) Percent distribution of DNA damage in L929 cells treated with varying concentrations of Mo-NPs for 24 h. Olive tail moment (OTM) values were determined following the algorithm (olive tail moment = (tail mean – head mean) tail% DNA/100) using Comet Assay IV software.

given mass and large specific surface area of NPs, they are capable of reaching the nucleus and interacting with DNA [56,57]. The mode of action may include the inhibition of various enzymes involved in DNA repair, expression, and possibly the induction of reactive oxygen species, which may inflict DNA damage. This DNA damage may either lead to carcinogenesis cell death or the disruption of normal cell functions. The DNA damage responses by comet assay are due to the exposure to various nanoparticles, which have been observed at this concentration range in human liver cells (HepG2) [41], human umbilical vein endothelial cells (HUVECs) [51], and in fish cells [58]. Our earlier studies have also revealed that titanium dioxide nanoparticles (TiO_2-NPs) and zinc ferrite nanoparticles ($ZnFe_2O_4$-NPs) can induce DNA damage in human amnion epithelial cells (WISH) as proven by the comet assay [14,40].

In conclusion, the present study, for the first time, demonstrated the cyto- and genotoxicity of Mo-NPs in L929 cell line. We have shown that Mo-NPs induced significant cytotoxicity in L929 cells in a concentration and time dependent manner. This nanocrystalline particle was also found to induce oxidative stress as observed by the induction of ROS generation and LPO level, and the depletion of GSH level and catalase activity. The decrease in mitochondrial membrane potential also confirms the impaired mitochondrial activity. This *in vitro* study also showed the induction of apoptosis in Mo-NPs exposed L929 cells through G2/M arrest and DNA damage. Thus, our findings suggest the potential hazardous nature of Mo-NPs.

Conflict of interest

The authors declare that they have no conflict of interest.

Acknowledgments

This work was supported by NSTIP Strategic Technologies Program number (12-MED2491-02) in the Kingdom of Saudi Arabia.

References

[1] U. Häfeli, W. Schütt, J. Teller, M. Zborowski, Plenum Press, New York (1997).
[2] V.L. Colvin, Nat. Biotechnol. 21 (2003) 1166.
[3] E. Oberdörster, Environ. Health Perspect. 112 (2004) 1058.

[4] I. Lynch, K.A. Dawson, S. Linse, Sci. STKE 327 (2006) 14.
[5] S. Foley, C. Crowley, M. Smaihi, C. Bonfils, B. Erlanger, P. Seta, C. Larroque, Biochem. Biophys. Res. Commun. 294 (2002) 116.
[6] N. Lewinski, V. Colvin, R. Drezek, Small 4 (2008) 26.
[7] C.M. Sayes, R. Wahi, P.A. Kurian, Y. Liu, J.L. West, K.D. Ausman, D.B. Warheit, V.L. Colvin, Toxicol. Sci. 92 (2006) 174.
[8] M. Ahamed, M.A. Siddiqui, M.J. Akhtar, I. Ahmad, A.B. Pant, H.A. Alhadlaq, Biochem. Biophys. Res. Commun. 396 (2010) 578.
[9] M.A. Siddiqui, M. Ahamed, J. Ahmad, M.A.M. Khan, J. Musarrat, A.A. Al-Khedhairy, S.A. Alrokayan, Food Chem. Toxicol. 50 (2012) 641.
[10] A.A. Shvedova, V. Castranova, E.R. Kisin, D. Schwegler-Berry, A.R. Murray, V.Z. Gandelsman, A. Maynard, P. Baron, J. Toxicol. Environ. Health A 66 (2003) 1909.
[11] C.W. Lam, J.T. James, R. McCluskey, R.L. Hunter, Toxicol. Sci. 77 (2004) 126.
[12] S.M. Hussain, A.K. Javorina, A.M. Schrand, H.M. Duhart, S.F. Ali, J.J. Schlager, Toxicol. Sci. 92 (2006) 456.
[13] R. Wahab, M.A. Siddiqui, Q. Saquib, S. Dwivedi, J. Ahmad, J. Musarrat, A.A. Al-Khedhairy, S.H. Shin, Colloids Surf. B: Biointerfaces 117 (2014) 267.
[14] Q. Saquib, A.A. Al-Khedhairy, M.A. Siddiqui, F.M. Abou-Tarboush, A. Azam, J. Musarrat, Toxicol. In Vitro 26 (2012) 351.
[15] M.A. Siddiqui, H.A. Alhadlaq, J. Ahmad, A.A. Al-Khedhairy, J. Musarrat, M. Ahamed, PLOS ONE 8 (2013) e69534.
[16] S. Dwivedi, M.A. Siddiqui, N.N. Farshori, M. Ahamed, J. Musarrat, A.A. Al-Khedhairy, Colloids Surf. B: Biointerfaces 122 (2014) 209.
[17] B. Fahmy, S.A. Cormier, Toxicol. In Vitro 23 (2009) 1365.
[18] L. Capasso, M. Camatini, M. Gualtieri, Toxicol. Lett. 226 (2014) 28.
[19] T. Paz-Elizur, Z. Sevilya, Y. Leitner-Dagan, D. Elinger, L.C. Roisman, Z. Livneh, Cancer Lett. 266 (2008) 60.
[20] M. Ahamed, M. Karns, M. Goodson, J. Rowe, S. Hussain, J. Schlager, Y. Hong, Toxicol. Appl. Pharmacol. 233 (2008) 404.
[21] F.K. Cobankara, H. Orucoglu, H.E. Ulker, C. Yildirim, M. Yalcin, A. Sengun, J. Paediatr. Dent. 1 (2013) 37.
[22] Y. Zheng, R. Li, Int. J. Mod. Phys. B 23 (2009) 1566.
[23] V.D.Z.P. Margriet, A.M. Neigh, J.J. de la F. de la, W.V. Henny, J.B. Jacob, L. Henk van, H. de, J. Wim, Biomaterials 32 (2011) 9810e9817.
[24] R. Rodulf, B. Friendrich, S. Stopic, I. Anzel, S. Tomic, M. Colic, J. Biomed. Appl. 26 (2012) 595.
[25] A.B. Pant, A.K. Agarwal, V.P. Sharma, P.K. Seth, Hum. Exp. Toxicol. 20 (2001) 412.
[26] M.A. Siddiqui, G. Singh, M.P. Kashyap, V.K. Khanna, S. Yadav, D. Chandra, A.B. Pant, Toxicol. In Vitro 22 (2008) 1681.
[27] M.A. Siddiqui, M.P. Kashyap, V. Kumar, A.A. Al-Khedhairy, J. Musarrat, A.B. Pant, Toxicol. In Vitro 6 (2010) 1592.
[28] J.A. Buege, S.D. Aust, Methods Enzymol. 52 (1978) 302.
[29] D. Chandra, K.V. Ramana, L. Wang, B.N. Christensen, A. Bhatnagar, S.K. Srivastava, Invest. Ophthalmol. Vis. Sci. 43 (2002) 2285.
[30] A.K. Sinha, Anal. Biochem. 47 (1972) 389.
[31] Y. Zhang, L. Jiang, L. Jiang, C. Geng, L. Li, J. Shao, L. Zhong, Chem-Bio. Inter. 189 (2011) 186.
[32] A.L. Patterson, Phys. Rev. 56 (1939) 978.
[33] A. Nel, T. Xia, L. Madler, N. Li, Science 311 (2006) 622.
[34] R.C. Murdock, L. Braydich-Stolle, A.M. Schrand, J.J. Schlager, S.M. Hussain, Toxicol. Sci. 101 (2008) 239.
[35] K.O. Yu, C.M. Grabinski, A.M. Schrand, R.C. Murdock, W. Wang, B. Gu, J.J. Schlager, S.M. Hussain, J. Nanopart. Res. 11 (2009) 15.
[36] S.M. Hussain, K.L. Hess, J.M. Gearhart, K.T. Geiss, J.J. Schlager, Toxicol. In Vitro 19 (2005) 975.
[37] L. Braydich-Stolle, S. Hussain, J.J. Schlager, M.C. Hofmann, Toxicol. Sci. 88 (2005) 412.
[38] M. Ahamed, M.J. Akhtar, M.A. Siddiqui, J. Ahmad, J. Musarrat, A.A. Al-Khedhairy, M.S. AlSalhi, S.A. Alrokayan, Toxicology 283 (2011) 101.
[39] J. Ahmad, M. Ahamed, M.J. Akhtar, S.A. Alrokayan, M.A. Siddiqui, J. Musarrat, A.A. Al-Khedhairy, Appl. Pharmacol. 259 (2012) 160, http://www.ncbi.nlm.nih.gov/pubmed/22245848Toxicol
[40] Q. Saquib, A.A. Al-Khedhairy, J. Ahmad, M.A. Siddiqui, S. Dwivedi, S.T. Khan, J. Musarrat, Toxicol. Appl. Pharmacol. 273 (2013) 289.
[41] V. Sharma, D. Anderson, A. Dhawan, Apoptosis 17 (2012) 852.
[42] H.K. Patra, S. Banerjee, U. Chaudhuri, P. Lahiri, A.K. Dasgupta, Nanomed.: Nanotechnol. Biol. Med. 3 (2007) 111.
[43] J. Ahmad, H.A. Alhadlaq, M.A. Siddiqui, Q. Saquib, A.A. Al-Khedhairy, J. Musarrat, M. Ahamed, Environ. Toxicol. (2013), http://dx.doi.org/10.1002/tox.21879.
[44] G. Sharma, V. Kodali, M. Gaffrey, W. Wang, K.R. Minard, N.J. Karin, J.G. Teeguarden, B.D. Thrall, Nanotoxicology 8 (2014) 663.
[45] K.M. Ramkumar, C. Manjula, G. Gnanakumar, M.A. Kanjwal, T.V. Sekar, R. Paulmurugan, P. Rajaguru, Eur. J. Pharm. Biopharm. 81 (2012) 324.
[46] K. Bhattacharya, P.C. Naha, I. Naydenova, S. Mintova, H.J. Byrne, Toxicol. Lett. 215 (2012) 151.
[47] R. Dornetshuber, P. Heffeter, M.R. Kamyar, T. Peterbauer, W. Berger, R. Lemmens-Gruber, Chem. Res. Toxicol. 20 (2007) 465.
[48] M.A. Siddiqui, J. Ahmad, N.N. Farshori, Q. Saquib, S. Jahan, M.P. Kashyap, M. Ahamed, J. Musarrat, A.A. Al-Khedhairy, Mol. Cell. Biochem. 384 (2013) 59.
[49] C.G. Ferreira, M. Epping, F.A. Kruyt, G. Giaccone, Clin. Cancer Res. 8 (2002) 2024.
[50] S. Huang, P.J. Chueh, Y.W. Lin, T.S. Shih, S.M. Chuang, Toxicol. Appl. Pharmacol. 241 (2009) 182.
[51] J. Duan, Y. Yu, Y. Li, Y. Yu, Y. Li, X. Zhou, P. Huang, Z. Sun, PLoS ONE 8 (2013) e62087.
[52] J. Wang, S. Engle, Y. Zhang, Cell Cycle 10 (2011) 500.
[53] P.V. AshaRani, G. Low Kah Mun, M.P. Hande, S. Valiyaveettil, ACS Nano 3 (2009) 279.
[54] H.J. Eom, J. Choi, Environ. Sci. Technol. 44 (2010) 8337.
[55] Y.S. Lee, D.W. Kim, Y.H. Lee, J.H. Oh, S. Yoon, M.S. Choi, S.K. Lee, J.W. Kim, K. Lee, C.W. Song, Arch. Toxicol. 85 (2011) 1529.
[56] C. Buzea, P. Blandino II, K. Robbie, Biointerphases 2 (2007) 17.
[57] X.J. Liang, C. Chen, Y. Zhao, L. Jia, P.C. Wang, Curr. Drug Metab. 9 (2008) 697.
[58] J.F. Reeves, S.J. Davies, N.J.F. Dodd, A.N. Jha, Mutat. Res. 640 (2008) 113.